Modal Shift Evaluation and Optimization for Resonance Mechanism Investigation and Mitigation of Power Systems Integrated with FCWG

Jianqiang Luo, Siqi Bu, *Senior Member, IEEE,* Jiebei Zhu, *Member, IEEE,* and C. Y. Chung, *Fellow, IEEE*

***Abstract*— The integration of full converter-based wind power generation (FCWG, e.g. permanent magnet synchronous generator (PMSG)) not only introduces the PMSG oscillation modes (POMs) but also might excite severe resonances with electromechanical oscillation modes (EOMs) of the power system. In this paper, a two-open-loop-subsystem dynamic model is firstly established to investigate the interactions between the PMSG and the rest of the power system. On this basis, a modal shift evaluation (MSE) method by using bilateral damping torque analysis is proposed to accurately quantify the interaction effect of POMs and EOMs on each other and effectively explain their complex interaction process. Then two important concepts, i.e., modal shift sensitivity (MSS) with respect to various PMSG controller parameters and resonance excitation index (REI) according to a per unit open-loop modal distance indicating the intensity of modal interactions, are derived to dig the essential modal resonance mechanisms. Furthermore, by using MSS and REI as two tools, the modal interaction optimization (MIO) is conducted through POM tuning in order to prevent potential system modal resonance and enhance resonance mode damping for the first time. The optimized modal interaction is validated to be beneficial and effective for the improvement of power system resonance stability.**

***Index Terms*-- PMSG, modal interaction, modal shift sensitivity (MSS), resonance excitation index (REI), POM tuning, resonance stability.**

I. Introduction

FULL converter-based wind power generation (FCWG) becomes increasingly favorable in wind generation market during recent years. The integration of wind power generation into power systems deteriorates the system dynamics and poses a critical threat to the system operation [1]-[6]. Although various control schemes have been applied in the wind power generation to improve the dynamic performance of the wind power generators [7]-[11], the dynamic interactions with power systems are much more complex to deal with. The resonance/oscillation events induced by wind power generation occur frequently and could result in a severe economic loss. On July 1, 2015, SSR took place in Xinjiang Province of China and led to the malfunction of protection and a huge power loss of 1280MW.

To address the dynamic impact of wind power generation and enhance the power system oscillatory stability, quite a few studies are conducted. The impact of the FCWG integration on power system stability can be assessed from two aspects, i.e., the power flow changes and the dynamic interactions. Reference [1] performs modal analysis to evaluate the overall impact, whilst reference [12] investigates the impact of variable speed wind generators on small-signal stability by using damping torque analysis (DTA), which can be a considerable improvement in understanding the overall impact. Reference [13] studies the small-signal stability of the FCWG in a sample system with lightly damped inter-area modes. It is concluded that the local and the park-level voltage controllers have the largest impact on the dominant inter-area mode. A stationary αβ-frame impedance model is developed in [14] to predict the stability impact of the PLL and coupling effect. An inclusive investigation of PI controller tuning is carried out in [15] so as to enhance the small-signal stability. As declared in [16], during the grid faults with type-4 wind turbines, the poorly damped mode may become unstable due to the interaction between PLL and alternating current control. The mechanism of the system instability conducted in [17] uses the 'positive feedback effect' between the electrical subsystem and the control subsystem to explain the dynamic process of instability brought by power converters.

The focus of the literature above is to examine the negative impact of FCWG integration on the power system dynamics mainly, whereas the more severe resonance caused by the modal interaction between the FCWG and main grid has not been fully investigated. An arresting phenomenon of strong modal resonance is introduced in [18] when two oscillatory modes are close in the frequency spectrum, and conclusions have been drawn that strong interaction may degrade the small-signal stability. Reference [19] demonstrates the strong resonance may lead to the oscillatory instability and the related eigenvalues change their size and direction when strong resonance happens. A general theory of interaction of eigenvalues is proposed in [20], where the strong and weak interactions are identified with their geometric interpretation on the complex plane. Reference [21] investigates the dynamic interactions brought by grid-connected PMSG and indicates that a modal resonance between EOM and POM may introduce a negative impact on small-signal stability. The PLL-induced modal resonance is further investigated in [22], finding that the dynamic impact of PLL may influence the dynamic performance of PMSG itself as well as the power system oscillation modes. However, the general modal interaction process between the FCWG and the power system electromechanical oscillation modes (EOMs) towards the strong resonance stage has not been thoroughly investigated in a quantitative manner, and hence their resonance mechanisms have not been fully revealed.

Considering all the points above, a novel modal shift evaluation methodology is proposed to quantify the impact of FCWG integration on power system resonance stability, which refers to the ability of the power system to prevent itself from the modal resonance during the modal interaction as the paper actually targets on more general modal interaction cases rather

than the previously-reported resonance studies on strong modal resonance only. The main contributions of this paper are: 1) A two-open-loop-subsystem dynamic model is developed, which divides the entire closed-loop power system into two open-loop subsystems, so that the dynamic impact of one subsystem on the other can be examined from either side; 2) A modal shift evaluation (MSE) method based on bilateral damping torque analysis (BDTA) is proposed to investigate the interaction effect of POMs and EOMs on each other and explain their complex interaction process, in which the linearization model for studying the modal impact on POMs from the external power system is proposed for the first time; 3) The modal shift sensitivity (MSS) is defined to examine the relationship between the PMSG controller parameters and the closed-loop modal shifts, and the accurate MSS can be used for modal interaction optimization (MIO). The resonance excitation index (REI) is also proposed to imply the intensity of modal interactions and plays as a valuable tool in the MIO; 4) Modal interaction, though as an unwanted phenomenon due to PMSG integration, is utilized to improve the resonance stability of the closed-loop power system for the first time. The model interaction optimization is achieved by properly tuning the PMSG controller parameters and hence the open-loop POM location.

The rest of the paper is organized as follows. Section II presents a two-open-loop-subsystem dynamic model, where a detailed 15th-order of PMSG is modeled as a subsystem and the rest of the power system is regarded as the other subsystem. In Section III, the MSE method is proposed based on BDTA. The concepts of modal shift sensitivity and resonance excitation index are also proposed. In Section IV, modal interaction analysis between POMs and EOMs is carried out, and the POM tuning method is implemented to optimize the modal interactions and thus improve system resonance stability, which is validated by time-domain simulations. Section V concludes this paper.

II. Two-Open-Loop-Subsystem Model

The physical structure of a PMSG connected to a multi-machine power system is shown in Fig. 1.

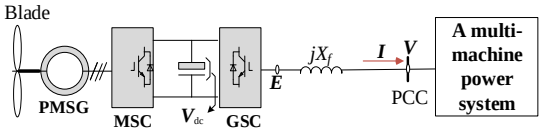

Fig.1. Configuration of a PMSG connected to a multi-machine power system.

To study the interactions between the PMSG and grid, a two-open-loop-subsystem dynamic model is proposed. With power flow profiles at the point of common coupling (PCC), two open-loop subsystems can be divided at PCC and derived with state space equations. Therefore, the open-loop modes of each subsystem can be examined separately.

A. Open-Loop Subsystem Model of PMSG

There are four main components in the subsystem with respect to the PMSG: 1) The PMSG; 2) The machine side converter (MSC) and the associated control system; 3) The DC-link, the grid side converter (GSC) and the associated control system; 4) The synchronous reference frame phase locked loop (SRF-PLL) which maintains the synchronization with the power system. Details of typical controller parameters and linearization of each component are given in [21].

The linearization equations of the open-loop PMSG subsystem can be expressed as

$$\begin{cases} \dfrac{d}{dt}\Delta \boldsymbol{X}_{pp} = \boldsymbol{A}_{gp}\Delta \boldsymbol{X}_{pp} + \boldsymbol{B}_{gp}\Delta \boldsymbol{V} \\ \Delta \boldsymbol{I} = \boldsymbol{C}_{gp}\Delta \boldsymbol{X}_{pp} + \boldsymbol{D}_{gp}\Delta \boldsymbol{V} \end{cases} \tag{1}$$

where $\Delta \boldsymbol{X}_{pp}$ is the vector of state variables of the PMSG including PLL. $\Delta \boldsymbol{V}=[\Delta V_x \quad \Delta V_y]^T$ is the voltage variation of PCC and $\Delta \boldsymbol{I}=[\Delta I_x \quad \Delta I_y]^T$ is current injection variation from PMSG at PCC under the common x-y coordinate system. $\boldsymbol{A}_{gp}$, $\boldsymbol{B}_{gp}$, $\boldsymbol{C}_{gp}$, $\boldsymbol{D}_{gp}$ denote the state space matrix of PMSG subsystem.

It is worth noting that $\boldsymbol{D}_{gp} = \boldsymbol{0}$ since d-axis and q-axis components of $\Delta \boldsymbol{I}$ are chosen as state variables, hence $\Delta \boldsymbol{I}$ can be expressed by $\Delta \boldsymbol{X}_{pp}$ without $\Delta \boldsymbol{V}$, which simplifies the formation of the closed-loop system state matrix.

Based on (1), the transfer function of the PMSG subsystem is obtained as

$$\boldsymbol{H}(s)=\Delta \boldsymbol{I} / \Delta \boldsymbol{V} = \boldsymbol{C}_{gp}(s\boldsymbol{I} - \boldsymbol{A}_{gp})^{-1}\boldsymbol{B}_{gp} \tag{2}$$

B. Open-Loop Subsystem Model of the Rest of the Power System

The state space model for N synchronous generators (SGs) in the rest of the power system can be written as

$$\begin{cases} \dfrac{d}{dt}\Delta \boldsymbol{X}_g = \boldsymbol{A}_g\Delta \boldsymbol{X}_g + \boldsymbol{B}_g\Delta \boldsymbol{V}_g \\ \Delta \boldsymbol{I}_g = \boldsymbol{C}_g\Delta \boldsymbol{X}_g + \boldsymbol{D}_g\Delta \boldsymbol{V}_g \end{cases} \tag{3}$$

where $\Delta \boldsymbol{X}_g$ denotes the vector of all the state variables of the N SGs. $\Delta \boldsymbol{I}_g$ and $\Delta \boldsymbol{V}_g$ are the SG terminal current injection variation and bus voltage variation at the connecting point. $\boldsymbol{A}_g$, $\boldsymbol{B}_g$, $\boldsymbol{C}_g$, $\boldsymbol{D}_g$ denote the state space matrix of the N SGs.

The linearization of the network equation is

$$\begin{bmatrix} \Delta \boldsymbol{I}_g \\ \Delta \boldsymbol{I} \end{bmatrix} = \boldsymbol{Y}\begin{bmatrix} \Delta \boldsymbol{V}_g \\ \Delta \boldsymbol{V} \end{bmatrix} = \begin{bmatrix} \boldsymbol{Y}_{ggN} & \boldsymbol{Y}_{gwN} \\ \boldsymbol{Y}_{wgN} & \boldsymbol{Y}_{wwN} \end{bmatrix}\begin{bmatrix} \Delta \boldsymbol{V}_g \\ \Delta \boldsymbol{V} \end{bmatrix} \tag{4}$$

where $\boldsymbol{Y}$ is the admittance matrix of the multi-machine power system with only the generator nodes.

Combining (3) and (4), the open-loop state space equations of the rest of the power system can be expressed as

$$\begin{cases} \dfrac{d}{dt}\Delta \boldsymbol{X}_g = \boldsymbol{A}_{gT}\Delta \boldsymbol{X}_g + \boldsymbol{B}_{gT}\Delta \boldsymbol{I} \\ \Delta \boldsymbol{V} = \boldsymbol{C}_{gT}\Delta \boldsymbol{X}_g + \boldsymbol{d}_I\Delta \boldsymbol{I} \end{cases} \tag{5}$$

where $\boldsymbol{A}_{gT}=\boldsymbol{A}_g+\boldsymbol{B}_g\left(\boldsymbol{Y}_{ggN}-\boldsymbol{Y}_{gwN}\boldsymbol{Y}_{wwN}^{-1}\boldsymbol{Y}_{wgN}-\boldsymbol{D}_g\right)^{-1}\boldsymbol{C}_g$,
$\boldsymbol{B}_{gT}=-\boldsymbol{B}_g(\boldsymbol{Y}_{ggN}-\boldsymbol{Y}_{gwN}\boldsymbol{Y}_{wwN}^{-1}\boldsymbol{Y}_{wgN}-\boldsymbol{D}_g)^{-1}\boldsymbol{Y}_{gwN}\boldsymbol{Y}_{wwN}^{-1}$,
$\boldsymbol{C}_{gT}=-\boldsymbol{Y}_{wwN}^{-1}\boldsymbol{Y}_{wgN}(\boldsymbol{Y}_{ggN}-\boldsymbol{Y}_{gwN}\boldsymbol{Y}_{wwN}^{-1}\boldsymbol{Y}_{wgN}-\boldsymbol{D}_g)^{-1}\boldsymbol{C}_g$,
$\boldsymbol{d}_I=\boldsymbol{Y}_{wwN}^{-1}+\boldsymbol{Y}_{wwN}^{-1}\boldsymbol{Y}_{wgN}(\boldsymbol{Y}_{ggN}-\boldsymbol{Y}_{gwN}\boldsymbol{Y}_{wwN}^{-1}\boldsymbol{Y}_{wgN}-\boldsymbol{D}_g)^{-1}\boldsymbol{Y}_{gwN}\boldsymbol{Y}_{wwN}^{-1}$.

The transfer function of the rest of power system is based on the state space matrix derived above, and hence it is very straightforward to obtain based on system linearization regardless of the system scale. Hence, based on (5), the open-loop transfer function of the rest of the power system is obtained as

$$\boldsymbol{G}(s)=\Delta \boldsymbol{V} / \Delta \boldsymbol{I}=[\boldsymbol{C}_{gT}(s\boldsymbol{I} - \boldsymbol{A}_{gT})^{-1}\boldsymbol{B}_{gT} + \boldsymbol{d}_I] \tag{6}$$

C. Closed-Loop Model of the Entire Power System

The closed-loop model of the entire power system can be derived by integrating two open-loop subsystems and shown in Fig. 2.

By dividing the entire system into two subsystems, the damping impact and mechanism of one subsystem on the other can be derived and analyzed, which is the essential cause of bilateral modal interactions/shifts between two subsystems and cannot be revealed by a complete closed-loop system.

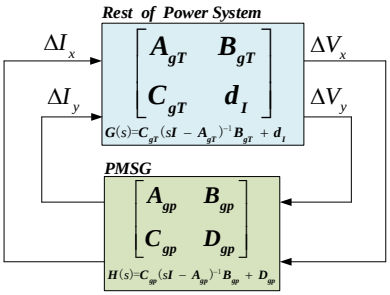

Fig. 2. The connection of two open-loop subsystems.

III. Modal Shift Evaluation and Optimization Methodology

Based on Section II, the closed-loop power system is formed by two open-loop subsystems. Each subsystem has a group of open-loop modes, i.e. the open-loop oscillation modes of PMSG (POMs), and the open-loop electromechanical oscillation modes (EOMs) of the rest of the power system. The interactions between POMs and EOMs cause the closed-loop modal shifts, which is carefully investigated in this section.

A. Bilateral Damping Torque Analysis

To investigate the bilateral modal interactions between EOMs and POMs, a bilateral damping torque analysis (BDTA) is proposed.

On one hand, when the subsystem of PMSG is investigated, the rest of the power system can be regarded as a voltage source which responses to the current variation of PMSG. On the other hand, when the rest of the power system is the main analysis focus, the subsystem of PMSG is regarded as a current source [23], which provides the grid supporting function for the power system and responses to the variation of PCC voltage. In other words, the entire system can be divided into two interactive subsystems. When one subsystem is studied, the other subsystem can be regarded as a controller with all the modes integrated into a two-by-two transfer function matrix (as shown in Fig. 2), and vice versa. The detailed procedures are presented as follows:

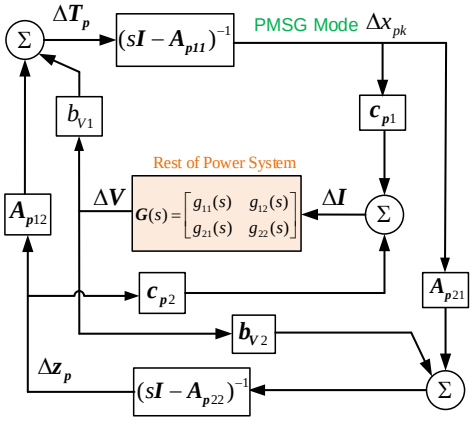

Fig. 3. Linearized model for contribution from the rest of the power system to PMSG mode.

First, we investigate the modal interaction from the rest of the power system to the subsystem of PMSG. By replacing the representation of the upper subsystem in Fig. 2 with its detailed transfer function $\boldsymbol{G}(s)$, a linearized model to quantify the contribution from the rest of the power system to POM shifts is derived and shown in Fig. 3. The PMSG mode mentioned in the diagram can refer to any PMSG mode like DC voltage control mode, PLL mode etc., which will be analyzed in the case study.

To perform BDTA, (1) is rearranged as

$$\frac{\boldsymbol{d}}{\boldsymbol{dt}}\begin{bmatrix}\Delta \boldsymbol{x_{pk}}\\ \Delta \boldsymbol{z_p}\end{bmatrix}=\begin{bmatrix}\boldsymbol{A}_{p11} & \boldsymbol{A}_{p12}\\ \boldsymbol{A}_{p21} & \boldsymbol{A}_{p22}\end{bmatrix}\begin{bmatrix}\Delta \boldsymbol{x_{pk}}\\ \Delta \boldsymbol{z_p}\end{bmatrix}+\begin{bmatrix}\boldsymbol{b}_{V1}\\ \boldsymbol{b}_{V2}\end{bmatrix}\Delta \boldsymbol{V}$$
$$\Delta \boldsymbol{I}=\begin{bmatrix}\boldsymbol{c}_{p1} & \boldsymbol{c}_{p2}\end{bmatrix}\begin{bmatrix}\Delta \boldsymbol{x_{pk}}\\ \Delta \boldsymbol{z_p}\end{bmatrix} \tag{7}$$

where Δx_{pk} is the k[th] state variable vector of $\Delta \boldsymbol{X_{pp}}$, and $\Delta \boldsymbol{z_p}$ is the rest of state variables in $\Delta \boldsymbol{X_{pp}}$.

As illustrated in Fig. 3, the rest of the power system is regarded as a two-input two-output controller, and thus its impact on the closed-loop PMSG mode can be assessed by damping torque analysis. The forward path from the rest of the power system to PMSG is

$$\frac{\Delta \boldsymbol{T_p}}{\Delta \boldsymbol{V}}=\boldsymbol{F_p}(s)=\boldsymbol{b}_{V1}+\boldsymbol{A}_{p12}(s\boldsymbol{I}-\boldsymbol{A}_{p22})^{-1}\boldsymbol{b}_{V2} \tag{8}$$

where ΔT_p is a quasi-damping torque which contributes the oscillation mode with respect to Δx_{pk}.

Assume $\lambda_{pi}=-\sigma_{pi}+j\omega_{pi}$ as the i[th] oscillation mode of PMSG, then $\Delta \boldsymbol{I}$ should be equal to $\gamma_{pik}\Delta x_{pk}$ [12].

Hence, the relationship between $\Delta \boldsymbol{T_p}$ and Δx_{pk} can be obtained

$$\Delta \boldsymbol{T_p}=\boldsymbol{F_p}(s)\boldsymbol{G}(s)\gamma_{\boldsymbol{pik}}(s)\Delta \boldsymbol{x_{pk}} \tag{9}$$

Let $s=\lambda_{pi}$ in the above equation, the damping torque provided by the rest of the power system to the k[th] mode of PMSG can be

$$\Delta \boldsymbol{T_p}=\boldsymbol{F_p}(\lambda_{\boldsymbol{pi}})\boldsymbol{G}(\lambda_{\boldsymbol{pi}})\gamma_{\boldsymbol{pik}}(\lambda_{\boldsymbol{pi}})\Delta \boldsymbol{x_{pk}} \tag{10}$$

The sensitivity of λ_{pi} with respect to the damping torque coefficient of the k[th] mode of PMSG, which refers to the relativity of Δx_{pk} to λ_{pi}, can be computed to be

$$S_{pik}=\frac{\partial \lambda_{\boldsymbol{pi}}}{\partial \boldsymbol{T_p}}=w_{pik}v_{pik} \tag{11}$$

where w_{pik} and v_{pik} are the elements in λ_{pi} associated left eigenvector $\boldsymbol{w_{pi}}$ and right eigenvector $\boldsymbol{v_{pi}}$ corresponding to $\Delta \boldsymbol{x_{pk}}$.

Thus, the variation of the i[th] eigenvalue λ_{pi} in PMSG caused by the dynamics of the rest of the power system can be assessed by employing S_{pik} [24, 25],

$$\Delta \lambda_{pi}=S_{pik}\boldsymbol{F_p}(\lambda_{pi})\boldsymbol{G}(\lambda_{pi})\gamma_{\text{pik}}(\lambda_{pi}) \tag{12}$$

Second, we also apply BDTA on the rest of the power system. The rearrangement of state equations (5) is expressed as

$$\frac{d}{dt}\begin{bmatrix}\Delta \boldsymbol{\delta}\\ \Delta \boldsymbol{\omega}\\ \Delta \boldsymbol{z}\end{bmatrix}=\begin{bmatrix}\boldsymbol{0} & \boldsymbol{\omega_0 I} & \boldsymbol{0}\\ \boldsymbol{A_{21}} & \boldsymbol{A_{22}} & \boldsymbol{A_{23}}\\ \boldsymbol{A_{31}} & \boldsymbol{A_{32}} & \boldsymbol{A_{33}}\end{bmatrix}\begin{bmatrix}\Delta \boldsymbol{\delta}\\ \Delta \boldsymbol{\omega}\\ \Delta \boldsymbol{z}\end{bmatrix}+\begin{bmatrix}\boldsymbol{0}\\ \boldsymbol{b_{I2}}\\ \boldsymbol{b_{I3}}\end{bmatrix}\Delta \boldsymbol{I}$$
$$\Delta \boldsymbol{V}=\begin{bmatrix}\boldsymbol{C_{g1}} & \boldsymbol{C_{g2}} & \boldsymbol{C_{g3}}\end{bmatrix}\begin{bmatrix}\Delta \boldsymbol{\delta}\\ \Delta \boldsymbol{\omega}\\ \Delta \boldsymbol{z}\end{bmatrix}+\boldsymbol{d_I}\Delta \boldsymbol{I} \tag{13}$$

Similar to Fig. 3, by replacing the representation of PMSG subsystem in Fig. 2 with its detailed transfer function $\boldsymbol{H}$(s), a linearized model to quantify the contribution from the subsystem of PMSG to EOM shifts is derived and shown in Fig. 4.

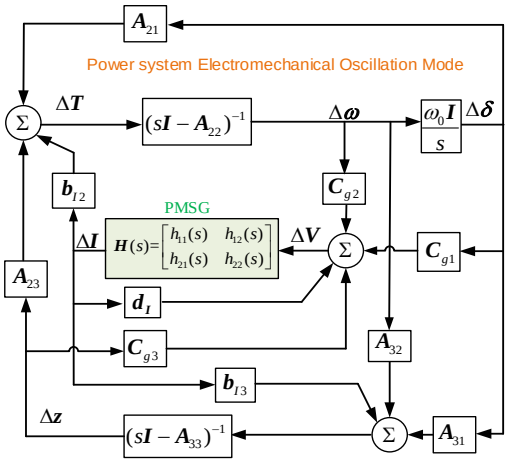

Fig. 4. Linearized model for contribution from PMSG to power system EOM

The forward path from PMSG to the rest of the power system is

$$\frac{\Delta \boldsymbol{T}}{\Delta \boldsymbol{I}} = \boldsymbol{F}(s) = \boldsymbol{b}_{I2} + \boldsymbol{A}_{23}(s\boldsymbol{I} - \boldsymbol{A}_{33})^{-1}\boldsymbol{b}_{I3} \tag{14}$$

Assume $\lambda_i = -\sigma_i + j\omega_i$ as the ith EOM of the rest of the power system, then $\Delta \boldsymbol{V}$ should be equal to $\gamma_{ik}\Delta\omega_k$ [12].

Hence, the relationship between damping torque $\Delta \boldsymbol{T}$ and $\Delta\omega_k$ can be obtained

$$\Delta \boldsymbol{T} = \boldsymbol{F}(s)\boldsymbol{H}(s)\gamma_{ik}(s)\Delta\omega_k \tag{15}$$

Let $s = \lambda_i$ in the above equation, the damping torque provided by PMSG to the $\Delta\omega_k$ (angular speed variation of kth SG) in the rest of the power system can be

$$\Delta \boldsymbol{T} = \boldsymbol{F}(\lambda_i)\boldsymbol{H}(\lambda_i)\gamma_{ik}(\lambda_i)\Delta\omega_k \tag{16}$$

The sensitivity of λ_i with respect to the damping torque coefficient of the kth SG in the rest of the power system can be computed to be

$$S_{ik} = \frac{\partial \lambda_i}{\partial \boldsymbol{T}} = w_{ik}v_{ik} \tag{17}$$

where w_{ik} and v_{ik} are the elements in λ_i associated left eigenvector $\boldsymbol{w_i}$ and right eigenvector $\boldsymbol{v_i}$ corresponding to $\Delta\omega_k$.

Therefore, the variation of the ith eigenvalue λ_i in the rest of the power system caused by the dynamics of PMSG can be assessed by employing S_{ik},

$$\Delta\lambda_i = \sum_{k=1}^{n} S_{ik}\boldsymbol{F}(\lambda_i)\boldsymbol{H}(\lambda_i)\gamma_{ik}(\lambda_i) \tag{18}$$

From (12) and (18), the closed-loop modal shifts are closely related to the transfer function $\boldsymbol{G}(s)$ and $\boldsymbol{H}$(s). Since λ_{pi} is one of the poles in $\boldsymbol{H}$(s), and λ_i is one of the poles in $\boldsymbol{G}(s)$, if $\lambda_{pi} \approx \lambda_i$, i.e. one of POMs is close to one of the EOMs, then both $G(\lambda_i)$ and $H(\lambda_{pi})$ would be very large, hence $\Delta\lambda_{pi}$ and $\Delta\lambda_i$ may also be large, which indicates large modal shifts may happen in the closed-loop system. The dynamic interaction process between two subsystems is thus evaluated by (12) and (18), which provides a quantitative understanding on the modal interaction process and set up a foundation for the modal shift evaluation (MSE) method.

Also, the analytical relationship in (12) and (18) can facilitate the optimization process, narrow the optimization search range and improve the optimization efficiency, which cannot be achieved by other parameter tuning methods such as root locus and Nyquist criteria.

B. Modal Shift Sensitivity

The modal shift sensitivity (MSS) is an index to measure the impact of modal interaction on closed-loop modal shifts with respect to the parameters of the controllers in PMSG, it can be defined as:

$$\text{MSS} = \frac{\Delta\lambda}{\Delta p} = S_i\boldsymbol{F}(\lambda_i)\boldsymbol{Tf}(\lambda_i)\gamma_i(\lambda_i)/\Delta p \tag{19}$$

where $\Delta\lambda$ is closed-loop modal shift, Δp is the controller parameter variation in PMSG. $\boldsymbol{Tf}$ denotes the transfer function of the subsystem, i.e, $\boldsymbol{G}(s)$ or $\boldsymbol{H}$(s).

MSS is an indicator to show how the control parameters contribute to the closed-loop modal shifts. It provides physical insights into how POMs interact with EOMs. MSS gives the accurate information of which parameter or controller is the key that can be used for optimization. From (19), MSS reveals which part of damping contribution (e.g. $S_i\boldsymbol{F}(\lambda_i)\boldsymbol{Tf}(\lambda_i)\gamma_i(\lambda_i)$) changes with the parameter and how it changes. Meanwhile, MSS is also influenced by the forward path function $\boldsymbol{F}$(s) which may vary under various operation conditions (e.g. power injection levels, different control strategies). Therefore, MSS plays an important role in deepening the understanding on resonance mechanism, which will be further examined in the case study.

C. Resonance Excitation Index

From the analysis above, the PMSG integration introduces modal interactions with EOMs of the power system. To quantify the intensity of the modal interactions, the resonance excitation index (REI) is proposed. It is defined as:

$$\text{REI} = \frac{\Delta d_{Closed}}{\Delta d_{open}} = \frac{|\lambda_{CEOM} - \lambda_{CPOM}|}{|\lambda_{EOM} - \lambda_{POM}|} \tag{20}$$

where $\Delta d_{Closed} = |\lambda_{CEOM} - \lambda_{CPOM}|$ is the Euclidian distance between closed-loop EOM and POM in the complex plane, and $\Delta d_{open} = |\lambda_{EOM} - \lambda_{POM}|$ is the Euclidian distance between open-loop EOM and POM in the complex plane.

If REI > 1, the modal interaction is repulsive, which indicates a weak resonance stability. The larger the REI is, the stronger the repulsion effect is. As a matter of convenience, when REI > 2, the repulsive interaction is identified to be 'strong' for modal resonance, which leads to large modal shifts of EOM and POM in mutually repulsive directions. When modal resonance happens, the damping of one mode becomes better and that of the other becomes worse as shown in Fig. 5(a), and thus the overall dynamic performance becomes worse [22].

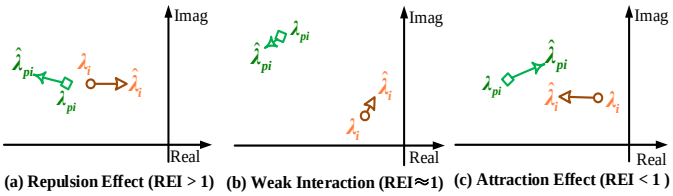

(a) Repulsion Effect (REI > 1) (b) Weak Interaction (REI≈1) (c) Attraction Effect (REI < 1)

Fig. 5. Potential movements of modal interactions.

If REI ≈ 1, the oscillation modal shifts are very small, which implies the modal interactions are quite weak as shown in Fig. 5(b), i.e. weak interaction.

If REI < 1, the closed-loop modes tend to move towards each other in an attractive manner, which indicates a strong resonance stability. The smaller the REI is, the stronger the attraction effect is. In this attraction effect, one mode becomes better and the other becomes worse as shown in Fig. 5(c), whereas the

overall dynamic performance is improved.

Therefore, REI can assess the intensity of modal interactions and acts as an inequality constraint in MIO so as to mitigate the potential negative effect on power system resonance stability.

D. Modal Interaction Optimization by POM Tuning

From the discussion above, the bilateral interactions between POMs and EOMs can be examined by BDTA, and the relationship with respect to PMSG controller parameters can be quantified by MSS.

To utilize the modal interactions between POMs and EOMs, a POM tuning method is proposed to improve the overall dynamic performance of the closed-loop system. There are five major steps in POM tuning:

(1) Identify the EOM;

(2) Identify the POMs and their related controllers;

(3) Calculate MSS, determine which POM and related controller parameters need to be tuned;

(4) Based on Step (2) & (3), tune the parameters of controllers according to the related controller and associated POM;

(5) Use time-domain simulations to verify the effectiveness of POM tuning.

To obtain the feasible parameters of PMSG controllers, the optimization problem can be defined as

$$\begin{aligned} &\text{Maximize} \quad F(p_i)=\min\{\xi_{CPOM}(p_i),\xi_{CEOM}(p_i)\} \\ &\textit{subject to} \quad p_l \le p_i \le p_h \qquad l,i,h=1,...,m \\ &\qquad\qquad \text{REI}(p_i)<1 \end{aligned} \tag{21}$$

where p_i are the parameters of PMSG controllers to be tuned, p_l and p_h are the low boundaries and high boundaries of p_i, $\xi_{CPOM}(p_i)$ and $\xi_{CEOM}(p_i)$ are the damping ratios of the closed-loop oscillation modes, and REI (p_i) is the resonance excitation index, which ensures the attraction effect in modal interactions.

Since the objective function (21) is not explicit, and the range of the controller parameters can be defined, it is a constrained optimization problem. A traditional particle swarm optimization (PSO) algorithm is implemented to optimize the PMSG controller parameters.

Based on analysis of A~D in section III, the procedure of the proposed methodology is illustrated in Fig. 6.

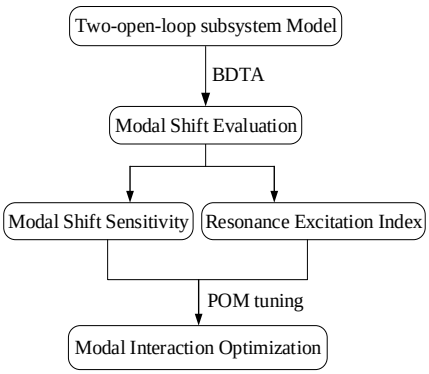

Fig. 6. Flowchart of modal shift evaluation and optimization methodology.

IV. Case Study

A. The Example Power System

Fig. 7 presents the configuration of example New England power system integrated with an FCWG wind farm connected at Bus 22 with P_{FCWG}=1.5p.u. The detailed 15th order PMSG with SRF-PLL dynamics is used and adopts the reactive power control with constant power factor (0.95). The simplified third-order model of the synchronous generators (SGs) and a first-order of the automatic voltage regulator (AVR) are adopted. The parameters of example system and typical controller parameters of a PMSG in [19] are used.

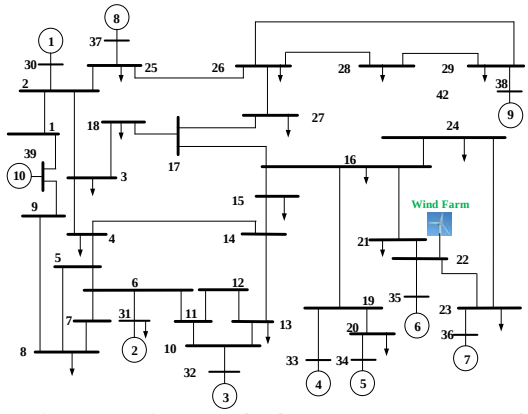

Fig. 7 Configuration of New England power system integrated with an FCWG wind farm.

The open-loop EOMs are calculated when the PMSG dynamics are excluded and PMSG is modeled as a constant current source. With the power flow profile at Bus 22, the open-loop modes of PMSG can also be calculated as shown in Table I.

TABLE I The Open-loop Modes of PMSG

Mode	λ_{pi}	Frequency	Damping ratio	Associated variables	Related controller
POM1	-2.5000 +22.2205i	3.54	0.1118	$\Delta\psi_{psd}$ Δx_{p3}	MSC d-axis current controller
POM2	-2.1846 +22.2055i	3.53	0.0979	$\Delta\psi_{psq}$ Δx_{p2}	MSC q-axis current controller
POM3	-0.3154 +1.5528i	0.25	0.1990	$\Delta\omega_{pr}$ Δx_{p1}	MSC rotor speed controller
POM4	-12.4712 +69.6210i	11.10	0.1764	ΔI_{pcd} Δx_{p5}	GSC d-axis current controller
POM5	-22.6548 +97.8699i	15.59	0.2255	ΔI_{pcq} Δx_{p7}	GSC q-axis current controller
POM6	-0.0370 +0.8208i	0.13	0.0451	ΔV_{pdc} Δx_{p4}	GSC DC voltage controller
POM7	-5.0198	0.00	1.0000	Δx_{p6}	GSC reactive power controller
POM8	-2.2290 +5.9008i	0.94	0.3534	Δx_{pll} $\Delta\theta_{pll}$	PLL controller

B. Validation of Modal Shift Evaluation Method

As stated in section III, the PMSG is denoted as a subsystem and the rest of the New England power system is regarded as the other subsystem. BDTA is employed on PMSG, and POM shifts are assessed as shown in Table II.

TABLE II Closed-Loop Modal Shift Evaluation on POMs

Mode	λ_{pi}	$\Delta\lambda_{pi}$	Predicted $\hat{\lambda}_{pi}$	Real $\hat{\lambda}_{pi}$
POM1	-2.5000 +22.2205i	0.0000 +0.0000i	-2.5000 +22.2205i	-2.5000 +22.2205i
POM2	-2.1846 +22.2055i	0.0000 +0.0000i	-2.1846 +22.2055i	-2.1846 +22.2055i
POM3	-0.3154 +1.5528i	0.0000 +0.0000i	-0.3154 +1.5528i	-0.3154 +1.5528i
POM4	-12.4712 +69.6210i	0.0001 +0.0001i	-12.4711 +69.6211i	-12.4713 +69.6210i
POM5	-22.6548 +97.8699i	0.0152 -0.0192i	-22.6396 +97.8507i	-22.6235 +97.8222i
POM6	-0.0370 +0.8208i	0.0009 -0.0003i	-0.0362 +0.8205i	-0.0365 +0.8205i
POM7	-5.0198	0.0500	-4.9799	-4.9709
POM8	-2.2290 +5.9008i	0.0091 +0.0199i	-2.2199 +5.9207i	-2.2132+ 5.9111i

Then BDTA is also performed on the rest of the power system. EOM shifts therefore can be predicted as shown in Table

III. There are 9 EOMs, only 3 typical EOMs are listed to save space.

TABLE III CLOSED-LOOP MODAL SHIFT EVALUATION ON EOMS

Mode	λ_i	$\Delta\lambda_i$	Predicted $\hat{\lambda}_i$	Real $\hat{\lambda}_i$
EOM1	-0.1795+ 3.1464i	0.0570 -0.0645i	-0.1225 +3.0818i	-0.1210 +3.0773i
EOM2	-1.4768 + 4.8566i	-0.0321 +0.0317i	-1.5088 +4.8883i	-1.5165 +4.8974i
EOM3	-0.1888 + 5.2954i	-0.0011 -0.0103i	-0.1899 +5.2851i	-0.1897 +5.2816i

From Table II and Table III, the predicted closed-loop modes and the real closed-loop modes are almost equal. This proves the effectiveness of the proposed evaluation method. In Table II, $\Delta\lambda_{pi}$*=0,i=1,2,3* , it supports the fact that the wind turbine modes (POM1~POM3) are decoupled from the power system by converters, which has been concluded in lots of literature. In Table III, $\Delta\lambda_{EOM3} = 0$, it proves that PMSG can only interact with the local mode of the same area and the inter-area mode, cannot impact other local modes.

It is worth pointing out that the two resonance-related modes are the main concern and they are not necessarily the dominant or critical modes of either system in the common sense. Other POMs (POM4~POM8) also interact with the rest of power system. However in normal cases, these interactions are quite weak or even can be ignored (i.e., the eigenvalue shifts are quite small). But if the controller parameters are not properly tuned, POM4~POM8 may induce strong interactions with other EOMs of the rest of power system and hence influence resonance stability.

C. Investigation of Modal Interaction Process

As shown in Table I, the POMs are closely related to its according controller parameters. Here we choose the PLL controller as an example to demonstrate the modal interaction between POM8 and EOM1.

By changing the proportional parameter K_{ppll}, POM8 moves horizontally as shown in Fig. 8. The open-loop EOM1 stays at a constant point, while the POM8 (the dark blue curve) moves from the right to the left. Hence, the two closed-loop oscillation modes can be calculated and classified to be closed-loop POM8 (CPOM8, the light blue curve) and the closed-loop EOM1 (CEOM1, the magenta curve).

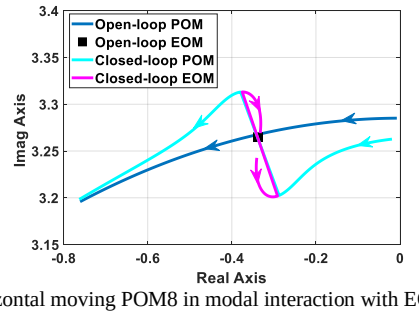

Fig. 8. Horizontal moving POM8 in modal interaction with EOM1.

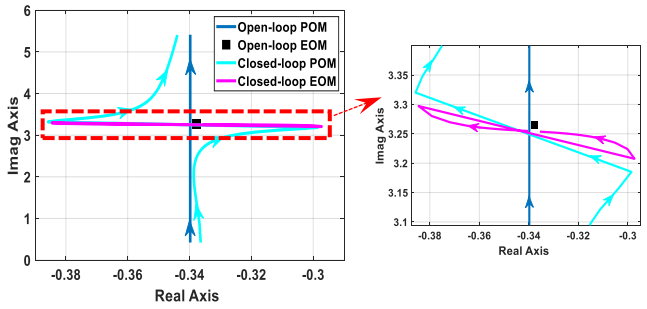

Fig. 9. Vertical moving POM8 in modal interaction with EOM1.

From the eigenvalue locus in Fig. 8, while the POM8 moves from the right and approaches towards EOM1, CEOM1 moves around EOM1. When POM8 is close to EOM1, the CEOM1 and CPOM8 exchanges the moving path to avoid moving too far from the open-loop modes. As POM8 moves away from EOM1, the closed-loop modal shifts decrease indicating that the modal interactions become weak. Hence, it can be concluded that the position of POM8 influences the position of CEOM1, especially when it is close to EOM1. The impact may be detrimental or beneficial for the system damping depending on its position.

By changing the integral parameter K_{ipll}, POM8 moves vertically as shown in Fig. 9. There is also a path exchange between CEOM1 and CPOM8 to keep CEOM1 moves near EOM1. When the distance between POM8 and EOM1 is large, the closed-loop modal shifts are very small, which indicates the modal interactions become weak. However, when the two open-loop modes are close, the strong modal interactions lead to a significant resonance, which makes a large modal shift from EOM1.

The horizontal approaching and vertical approaching movements demonstrate the modal interactions between POM8 and EOM1. There are also other approaching directions can be examined, which are not studied here due to the limit of space. Again, the strong modal resonance happens when the open-loop modes are close, which illustrates the modal interaction process between PMSG and the rest of the power system.

D. Sensitivity Analysis based on MSS

Since the inter-area mode λ_{EOM1} is the main concern of the power system, the MSS with EOM1 and POMs are calculated in Table IV.

TABLE IV
MODAL SHIFT SENSITIVITY WITH RESPECT TO PMSG CONTROLLER PARAMETERS

PMSG controllers	Parameter	MSS on EOM1	MSS on POMs
MSC rotor speed controller	K_{pp1}	-2.1572e-15 - 4.2178e-15i	-0.0640 - 0.0137i
	K_{pi1}	-3.3598e-15 - 2.7263e-15i	-0.0002 + 0.0378i
MSC d-axis current controller	K_{pp2}	-5.3710e-16 + 3.3712e-15i	-2.3511 - 0.3862i
	K_{pi2}	4.5201e-16 + 2.0317e-15i	-0.0001 + 0.1725i
MSC q-axis current controller	K_{pp3}	-2.7362e-15 + 2.0168e-15i	-2.6314 - 0.4321i
	K_{pi3}	-7.3128e-15 + 8.1569e-16i	0.0000 + 0.1322i
GSC DC voltage controller	K_{pp4}	**-7.4219e-05 + 5.3209e-05i**	-0.0172 - 0.0008i
	K_{pi4}	**-1.3274e-05 - 3.1726e-05i**	-0.0001 + 0.0218i
GSC d-axis current controller	K_{pp5}	2.1963e-08 - 4.2317e-08i	-28.3612 - 8.6347i
	K_{pi5}	2.1058e-08 + 6.8542e-09i	-0.0000 + 0.4211i
GSC reactive power controller	K_{pp6}	**-3.1027e-04 +5.4217e-05i**	1.2387 + 0.2721i
	K_{pi6}	**-2.9657e-05 - 8.1527e-05i**	-0.4862+0.0002i
GSC q-axis current controller	K_{pp7}	3.9521e-08 - 4.1275e-08i	-53.1274-23.4162i
	K_{pi7}	2.0174e-08+2.1066e-08i	0.0001 + 0.4821i
PLL controller	K_{ppll}	**-8.6954e-05 + 4.3522e-05i**	-0.5073 - 0.2122i
	K_{ipll}	**-2.0185e-05 - 2.6733e-05i**	0.0005 + 0.0921i

From the MSS in the third column, the impact from PMSG parameters to EOM1 can be measured, and MSS in the fourth column reflects the impact from PMSG parameters to the newly introduced POMs. Based on the numerical values shown in Table IV, the GSC DC voltage controller, GSC reactive power controller, and the PLL controller are identified to have stronger interactions than other controllers.

From the perspective of system operators, the EOMs are the main concern. The impact of PMSG controller parameters on

EOMs are examined for demonstration purposes here and surely the sensitivity analysis can be conducted in the opposite direction based on the BDTA. According to (19), the MSS with respect to EOMs is proportional to the transfer function $\boldsymbol{H}(s)$ of the PMSG subsystem. It is to be noted that the oscillation frequency range of EOMs is usually 0.2Hz ~ 2.0Hz (i.e. 1.26rad/s ~ 12.57rad/s). Since $\boldsymbol{H}(s)$ is a two-by-two transfer function matrix, two singular values response curves within this range can be drawn in Fig. 10. Under weak interaction condition, the singular values of $\boldsymbol{H}(s)$ are quite flat, whereas if PMSG controller parameters change to certain values (as denoted by purple curve), there is a peak resonance at ω=3.15rad/s in one response curve that indicates strong resonance may also happen in modal interactions at such frequency (e.g. EOM1).

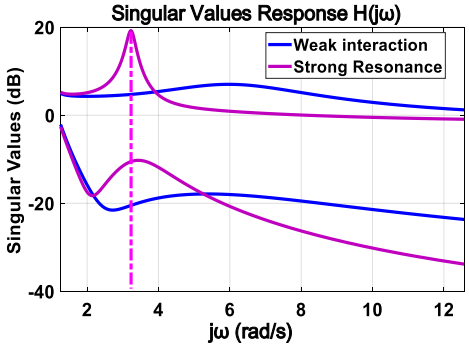

Fig. 10. Singular values response of $\boldsymbol{H}(s)$

Hence, MSS provides a clear insight of how PMSG controller parameters contribute to the closed-loop modal shifts and thus a deep understanding of resonance mechanism can be acquired. The analysis results can also effectively guide the MIO by POM tuning in the next subsection.

E. Modal Interaction Optimization and Effectiveness Analysis

As discussed above, modal interactions can be utilized to improve the dynamic performance of resonance EOM if proper tuning on POM is implemented.

Based on MSS, the POM8 is chosen to be tuned. Denote damping ratios of CPOM8 and CEOM1 as ξ_{CPOM8} and ξ_{CEOM1}. The overall dynamic performance can be implied by $\xi_{Csys} = \min\{\xi_{CEOM1}, \xi_{CPOM8}\}$.The optimization of the objective function is set as: Max $F = \xi_{Csys}$. The POM tuning based on PSO is carried out on the sample system, where the different modal interactions are compared, as shown in Table V.

TABLE V
POM TUNING ON PLL MODE

Interaction Type	Weak interaction	Strong Resonance	Optimized POM tuning
PLL parameters	K_{ppll}=4.4 K_{ipll}=39.27	K_{ppll}=0.24 K_{ipll}=10.30	K_{ppll}=0.82 K_{ipll}=6.65
POM8	-2.2317+5.9038i	-0.1217+3.2301i	-0.4174+2.5641i
CPOM8 (damping ratio)	-2.1836+5.9364i (34.52%)	-0.2504+3.3434i (7.47%)	-0.3775+2.5762i (14.50%)
EOM1	-0.1795+3.1464i	-0.1795+3.1464i	-0.1795+3.1464i
CEOM1 (damping ratio)	-0.1210+3.0773i (3.93%)	-0.0344+2.9740i (1.16%)	-0.2074+3.0759i **(6.73%)**
REI	1.0257	4.2069	0.8392
The intensity of modal interaction	Almost neutral	Strong repulsion effect	Considerable attraction effect

If strong modal resonance happens, the damping ratio of the resonance EOM decreases from 3.93% to 1.16%, which indicates that the modal resonance deteriorates the stability of the power system. However, after POM tuning, the damping ratio increases to **6.73%**, almost twice of that in weak interactions. REI=0.8392 <1 also indicates that the attraction effect helps improve the overall performance, as stated in section III.

To further validate the effectiveness of POM tuning, the time-domain simulations are also carried out. Three groups of different parameters in PLL are compared. The typical parameters in [19] are identified and denoted as weak interaction condition; if the PLL are not properly tuning, as stated in [20], modal resonance may be induced, which is set as the strong resonance condition. In addition, the optimal parameters obtained by the proposed POM tuning method are also used, which is named as the optimized POM tuning condition. The other parameters of PMSG and the rest of power system as well as the operation points are set to be the same in the time domain simulations. The disturbance is set to be: at t=0.2s, a three-phase to earth short circuit occurs at Bus 1 and subsequently clears after 100ms. The dynamic performance of closed-loop EOM1 and POM8 are shown in Fig. 11. Compared with the typical parameters in the base case (weak interaction condition), with optimized parameters in PLL, it is noteworthy that CEOM1 is improved while CPOM8 also has acceptable damping ratio, which is compliant with eigenvalue data in Table V. At the same time, the strong resonance condition encounters the worst dynamic performance, which may lead to instability. Once it is identified to be strong resonance condition, the POM tuning can also be implemented to ameliorate the situation. Therefore, MIO is capable to enhance the resonance stability of the power system.

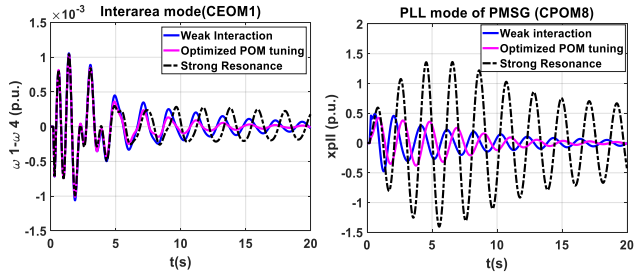

Fig. 11. Dynamic performance comparison of CEOM1 and CPOM8 under different modal interaction intensity.

The bus voltage and active power output at PCC and SG1 are illustrated in Fig. 12. If the PLL parameters are not properly tuned, strong resonance may deteriorate the damping of system and threaten the resonance stability. With optimized POM tuning, not only the strong resonance can be eliminated, but also the damping of system can be greatly enhanced. The time domain responses of the important variables related to PMSG and SGs are improved, indicating that the overall dynamic performance of the closed-loop power system is meliorated.

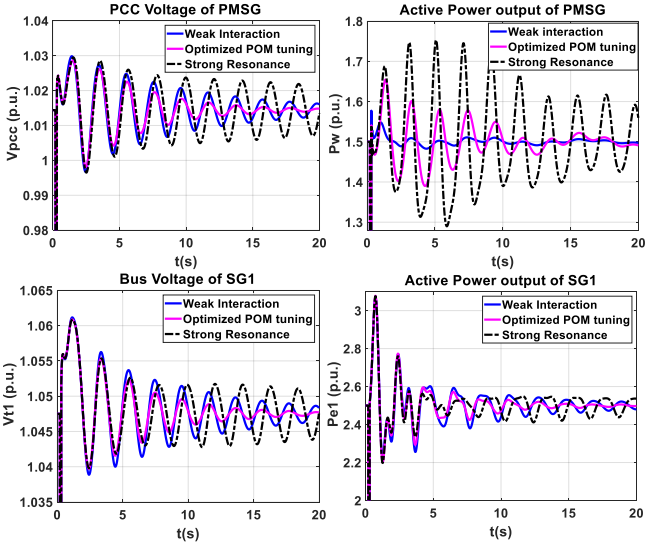

Fig. 12 Dynamic performance comparison of PMSG and SG1 with different PLL parameters.

TABLE VI
DAMPING IMPACT UNDER DIFFERENT WIND POWER PENETRATION LEVELS

Type	P (p.u.)	0.0	0.5	1.5	2.5	3.5
Weak interaction	CEOM1	-0.1537 +3.1235i	-0.1434 +3.1084i	-0.1210 +3.0773i	-0.0964 +3.0446i	-0.0695 +3.0101i
	DPI	NA	-0.6%	-0.65%	-0.70%	-0.74%
Strong resonance	CEOM1	-0.1537 +3.1235i	-0.0853 +3.0614i	-0.0344 +2.9740i	-0.0000 +2.9060i	**0.0288 +2.8454i**
	DPI	NA	-4.24%	-2.50%	-1.96%	-1.69%
Optimized POM tuning	CEOM1	-0.1537 +3.1235i	-0.1620 +3.1313i	-0.2074 +3.0759i	-0.2528 +3.0433i	-0.3086 +3.0150i
	DPI	NA	0.52%	1.21%	1.35%	1.29%

The penetration level of wind power generation also influences the intensity of modal interactions. With more wind power injected into the power system, the impact of PMSG on the rest of power system also grows (negative impact for strong resonance and positive for optimized POM tuning). A damping power index (DPI) is proposed to measure the damping enhancement after MIO with respect to different wind power penetration levels, which is defined as: $\mathrm{DPI} = (\zeta_{CEOM1} - \zeta_{EOM1})/P$, where ζ_{CEOM1} and ζ_{EOM1} are the damping ratios of CEOM1 and EOM1, and P represents the power injection from PMSG. From the definition, if DPI>0, the power injection benefits system damping, otherwise degrades system damping. Comparison of DPI with different power injections and optimized parameters is shown in Table VI. It can be demonstrated that for optimized POM tuning condition, under different penetration levels, the DPI is positive, and increases from 0.52% to 1.29%, which means the higher power injection, the higher DPI and the larger damping of the closed-loop power system. On the contrary, for strong resonance condition, the DPI stays at a big negative value with the increasing power injection, which indicates that strong resonance significantly exasperates the power system stability. Especially, the entire system becomes unstable when P=3.5. For the weak interaction condition, the DPI is a smaller negative value that indicates the weak interaction also degrades system damping but in a relatively slighter manner. Above all, the optimized modal interactions work effectively when operational condition varies, which validates the effectiveness of the MIO.

V. CONCLUSION

The impact of the FCWG integration on power system resonance stability has been investigated in this paper. By dividing the whole system into two subsystems, the modal interaction can be studied separately by regarding one subsystem as a two-input two-output controller while studying the other one. The bilateral damping torque analysis is employed to evaluate the closed-loop modal shifts with respect to different EOMs and POMs. The modal shift sensitivity and resonance excitation index provides physical insights into the impact on resonance modes with physical controllers and the intensity of modal interactions. Hence, a more specific parameter tuning can be implemented in related controllers to optimize the dynamic performance.

It is revealed that modal interactions do not necessarily deteriorate the system resonance stability. The impact can be evaluated with the proposed MSE method to determine whether measures should be taken to avoid the detrimental modal resonance. Therefore, the modal interactions can be utilized to improve the resonance EOM with acceptable POM, which indicates extra damping of EOM can be achieved with the proper tuning of PMSG controller parameters without auxiliary devices installed.

VI. ACKNOWLEDGMENT

The authors would like to acknowledge the support from National Natural Science Foundation of China for the Research Project (51807171), Guangdong Science and Technology Department for the Research Project (2019A1515011226), Hong Kong Research Grant Council for the Research Projects (25203917), (15200418) and (15219619), and Department of Electrical Engineering, The Hong Kong Polytechnic University for the Start-up Fund Research Project (1-ZE68).

VII. REFERENCES

[1] J. Quintero, V. Vittal, G. T. Heydt, and H. Zhang, "The Impact of Increased Penetration of Converter Control-Based Generators on Power System Modes of Oscillation," *IEEE Transactions on Power Systems*, vol. 29, no. 5, pp. 2248-2256, 2014.

[2] X. Xi, H. Geng, and G. Yang, "Small signal stability of weak power system integrated with inertia tuned large scale wind farm," in *2014 IEEE Innovative Smart Grid Technologies-Asia (ISGT ASIA)*, 2014, pp. 514-518: IEEE.

[3] L. P. Kunjumuhammed, B. C. Pal, R. Gupta, and K. J. Dyke, "Stability Analysis of a PMSG-Based Large Offshore Wind Farm Connected to a VSC-HVDC," *IEEE Transactions on Energy Conversion*, vol. 32, no. 3, pp. 1166-1176, 2017.

[4] J. Fang, H. Li, Y. Tang, and F. Blaabjerg, "On the Inertia of Future More-Electronics Power Systems," *IEEE Journal of Emerging and Selected Topics in Power Electronics*, pp. 1-1, 2018.

[5] W. Du, J. Bi, T. Wang, and H. Wang, "Impact of grid connection of large-scale wind farms on power system small-signal angular stability," *CSEE Journal of Power Energy Systems*, vol. 1, no. 2, pp. 83-89, 2015.

[6] W. Du, J. Bi, and H. Wang, "Small-signal angular stability of power system as affected by grid-connected variable speed wind generators-A survey of recent representative works," *CSEE Journal of Power Energy Systems*, vol. 3, no. 3, pp. 223-231, 2017.

[7] F. R. Badal, P. Das, S. K. Sarker, and S. K. Das, "A survey on control issues in renewable energy integration and microgrid," *Protection and Control of Modern Power Systems*, vol. 4, no. 1, p. 8, 2019.

[8] O. Carranza, E. Figueres, G. Garcerá, and R. Gonzalez-Medina, "Analysis of the control structure of wind energy generation systems based on a permanent magnet synchronous generator," *Applied Energy*, vol. 103, pp. 522-538, 2013.

[9] F. Wu, X. P. Zhang, and P. Ju, "Small signal stability analysis and control of the wind turbine with the direct-drive permanent magnet generator integrated to the grid," *Electric Power Systems Research*, vol. 79, no. 12, pp. 1661-1667, 2009.

[10] O. Noureldeen and I. Hamdan, "Design of robust intelligent protection technique for large-scale grid-connected wind farm," *Protection and Control of Modern Power Systems*, vol. 3, no. 1, p. 17, 2018.

[11] S. Li, T. A. Haskew, R. P. Swatloski, and W. Gathings, "Optimal and Direct-Current Vector Control of Direct-Driven PMSG Wind Turbines," *IEEE Transactions on Power Electronics*, vol. 27, no. 5, pp. 2325-2337, 2012.

[12] S. Q. Bu, X. Zhang, J. B. Zhu, and X. Liu, "Comparison analysis on damping mechanisms of power systems with induction generator based wind power generation," *International Journal of Electrical Power & Energy Systems*, vol. 97, pp. 250-261, 2018.

[13] T. Knüppel, J. N. Nielsen, K. H. Jensen, A. Dixon, and J. Ostergaard, "Small-signal stability of wind power system with full-load converter interfaced wind turbines," *IET Renewable Power Generation*, vol. 6, no. 2, 2012.

[14] X. Wang, L. Harnefors, and F. Blaabjerg, "Unified Impedance Model of Grid-Connected Voltage-Source Converters," *IEEE Transactions on Power Electronics*, vol. 33, no. 2, pp. 1775-1787, 2018.

[15] Y.-S. Kim, I.-Y. Chung, and S.-I. Moon, "Tuning of the PI Controller Parameters of a PMSG Wind Turbine to Improve Control Performance under Various Wind Speeds," *Energies*, vol. 8, no. 2, pp. 1406-1425, 2015.

[16] J. Hu, Q. Hu, B. Wang, H. Tang, and Y. Chi, "Small Signal Instability of PLL-Synchronized Type-4 Wind Turbines Connected to High-Impedance AC Grid During LVRT," *IEEE Transactions on Energy Conversion*, vol. 31, no. 4, pp. 1676-1687, 2016.

[17] S. Zhao and B. Shao, "An analytical method suitable for revealing the instability mechanism of power electronics dominated power systems,"

International Journal of Electrical Power & Energy Systems, vol. 109, pp. 269-282, 2019.
[18] K. R. Padiyar and H. V. SaiKumar, "Investigations on Strong Resonance in Multimachine Power Systems With STATCOM Supplementary Modulation Controller," *IEEE Transactions on Power Systems*, vol. 21, no. 2, pp. 754-762, 2006.
[19] I. Dobson, J. Zhang, S. Greene, H. Engdahl, and P. W. Sauer, "Is strong modal resonance a precursor to power system oscillations?," *IEEE Transactions on Circuits and Systems I: Fundamental Theory and Applications*, vol. 48, no. 3, pp. 340-349, 2001.
[20] A. P. Seyranian and A. A. Mailybaev, "Interaction of eigenvalues in multi-parameter problems," *Journal of Sound and Vibration*, vol. 267, no. 5, pp. 1047-1064, 2003.
[21] W. Du, X. Chen, and H. F. Wang, "Power System Electromechanical Oscillation Modes as Affected by Dynamic Interactions From Grid-Connected PMSGs for Wind Power Generation," *IEEE Transactions on Sustainable Energy*, vol. 8, no. 3, pp. 1301-1312, 2017.
[22] W. Du, X. Chen, and H. Wang, "PLL-Induced Modal Resonance of Grid-Connected PMSGs With the Power System Electromechanical Oscillation Modes," *IEEE Transactions on Sustainable Energy*, vol. 8, no. 4, pp. 1581-1591, 2017.
[23] J. Rocabert, A. Luna, F. Blaabjerg, and P. Rodríguez, "Control of Power Converters in AC Microgrids," *IEEE Transactions on Power Electronics*, vol. 27, no. 11, pp. 4734-4749, 2012.
[24] S. Bu, W. Du, and H. Wang, "Model validation of DFIGs for power system oscillation stability analysis," *IET Renewable Power Generation*, vol. 11, no. 6, pp. 858-866, 2017.
[25] M. J. Gibbard, D. Vowles, and P. Pourbeik, *Small-signal stability, control and dynamic performance of power systems*. University of Adelaide press, 2015.

VIII. Biography

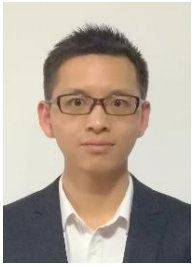

Jianqiang LUO received the B.Eng. and M.Eng. in electrical engineering all from Huazhong University of Science and Technology, Wuhan, China, in 2010 and 2015, respectively. He is a National Registered Electrical Engineer and Intermediate Economist in China. He is currently pursuing PhD in the Department of Electrical Engineering, Hong Kong Polytechnic University, Kowloon, Hong Kong SAR. He is also a visiting student with the Control and Power Laboratory, Imperial College London. His research involves power system stability analysis and control integrated with renewable energy.

Siqi Bu (S'11-M'12-SM'17) received the Ph.D. degree from the electric power and energy research cluster, The Queen's University of Belfast, Belfast, U.K., in 2012, where he continued his postdoctoral research work before entering industry. Then he was with National Grid UK as an experienced UK National Transmission System Planner and Operator. He is an Assistant Professor with The Hong Kong Polytechnic University, Kowloon, Hong Kong, and also a Chartered Engineer with UK Royal Engineering Council, London, U.K.. His research interests are power system stability analysis and operation control, including wind power generation, PEV, HVDC, FACTS, ESS and VSG.

He is an Associate Editor of IEEE Access and CSEE Journal of Power and Energy Systems, a Guest Editor of IET Renewable Power Generation and Energies, and an Editor of IEEE Open Access Journal of Power and Energy and Protection and Control of Modern Power Systems. He has received various prizes due to excellent performances and outstanding contributions in operational and commissioning projects during the employment with National Grid UK. He is also the recipient of Outstanding Reviewer Awards from IEEE Transactions on Sustainable Energy, IEEE Transactions on Power Systems, Applied Energy, Renewable Energy, International Journal of Electrical Power & Energy Systems and Journal of Modern Power System and Clean Energy respectively.

Jiebei Zhu (M'13) received the B.S. degree in microelectronics from Nankai University, Tianjin, China, in 2008, and the M.S. and Ph.D. degrees in electronic and electrical engineering from the University of Strathclyde, Glasgow, U.K., in 2009 and 2013, respectively.

He is currently a professor with the School of Electrical Automation and Information Engineering in Tianjin University. From 2013, he acts as a Senior Power System Engineer and Innovation Project Manager with National Grid Plc. of the GB transmission system operator. His research interests involve with HVDC transmission system control, renewable energy systems, and energy storage technologies.

Dr. Zhu was awarded with the license of "Chartered Engineer" by UK Engineering Council and IET.

C. Y. Chung (M'01-SM'07-F'16) received the B.Eng. (with First Class Honors) and Ph.D. degrees in electrical engineering from The Hong Kong Polytechnic University, Hong Kong, China, in 1995 and 1999, respectively.

Dr. Chung is currently a Professor, the NSERC/SaskPower (Senior) Industrial Research Chair in Smart Grid Technologies, and the SaskPower Chair in Power Systems Engineering with the Department of Electrical and Computer Engineering at the University of Saskatchewan, Saskatoon, SK, Canada.

Dr. Chung is an Editor of IEEE TRANSACTIONS ON POWER SYSTEMS, IEEE TRANSACTIONS ON SUSTAINABLE ENERGY, and IEEE POWER ENGINEERING LETTERS. He is also an IEEE PES Distinguished Lecturer.